Direct cationization of citrate-coated gold and silver nanoparticles

Marianna Barbalinardo,[a] Guido Ori,[b,c] Lisa Lungaro,[d] Giacomo Caio,[d] Andrea Migliori,[e] and Denis Gentili[,a]*

a) Consiglio Nazionale delle Ricerche, Istituto per lo Studio dei Materiali Nanostrutturati (CNR-ISMN), via P. Gobetti 101, 40129 Bologna, Italy
b) Université de Strasbourg, CNRS, Institut de Physique et Chimie des Matériaux de Strasbourg, UMR 7504, Rue du Loess 23, F-67034 Strasbourg, France
c) ADYNMAT CNRS consortium, F-67034 Strasbourg, France
d) Department of Translational Medicine, St. Anna Hospital, University of Ferrara, 44124 Ferrara, Italy
e) Consiglio Nazionale delle Ricerche, Istituto per la Microelettronica e Microsistemi (CNR-IMM), via P. Gobetti 101, 40129 Bologna, Italy

Keywords: nanoparticles, ligand exchange, cationization, surface chemistry, nanotoxicity in cells

Abstract

Nanoparticles have emerged as promising materials for a wide range of applications, including biomedicine, energy, and electronics. However, controlling their surface chemistry is essential to fully harness their potential, as it affects their physicochemical properties, stability, and interactions with biological systems. Surface functionalization is a key process enabling the adaptation of nanoparticle properties for specific applications. While introducing ligands during nanoparticle synthesis may not always be feasible, ligand exchange offers versatility in controlling surface chemistry. However, the direct replacement of negatively charged citrate on gold and silver nanoparticles with positive counterparts often leads to particle aggregation. Here, we present a straightforward one-step ligand exchange method to functionalize citrate-coated gold and silver nanoparticles with cationic ligands. By controlling citrate molecule protonation, we prevent nanoparticle aggregation, enabling successful displacement with positively charged alkanethiol ligands. Dynamic light scattering, zeta potential

measurement, transmission electron microscopy alongside theoretical models provide comprehensive insights into the mechanism and dynamics of ligand exchange. Furthermore, we demonstrate the impact of surface functionalization of nanoparticles on the cytotoxic activity of nanoparticles in model cell lines, underscoring the significance of surface chemistry of nanoparticles for their biomedical applications.

Introduction

Nanoparticles have emerged as promising materials for a wide range of applications, including biomedicine, energy, and electronics.[1-4] Yet, to unlock their full potential, precise control over their surface chemistry is imperative. Surface chemistry significantly influences their physicochemical characteristics, stability, and interactions with biological systems. Hence, surface functionalization emerges as a pivotal process, enabling tailoring of their properties to suit specific application requirements. The manipulation of nanoparticle surface chemistry can occur during synthesis or post-synthesis. During synthesis, this control is achieved by incorporating specific ligands into the reaction mixture alongside nanoparticle precursors. Alternatively, post-synthesis, the process involves ligand exchange, wherein the original ligands are displaced by new ones with a higher affinity for the nanoparticle surface.[5, 6]

The introduction of ligands during nanoparticle synthesis may not always be feasible due to incompatibility with the reactants or reaction conditions or because they may affect the size and shape of the resulting nanoparticles, leading to the formation of unwanted nanoparticles. On the other hand, ligand exchange is a more versatile strategy for controlling the surface chemistry of nanoparticles and, therefore, widely used to control their physical, chemical, and biological properties. For instance, we have successfully utilized ligand exchange to control the assembly of gold nanoparticles (AuNPs)[7] and to modulate the interaction of silver nanoparticles (AgNPs) with biomolecules and, in turn, their biological activity.[8-10] The most commonly used method for synthesizing AuNPs is the citrate

reduction technique, which allows for the controlled production of spherical nanoparticles.[11-13] These NPs are stabilized by electrostatic repulsions, which result from the negatively charged citrate molecules bound to their surface.[14, 15] Similarly, AgNPs are commonly synthesized in the presence of citrate molecules,[16, 17] serving as a stabilizing agent by imparting a negative surface charge to the nanoparticles. Despite its utility, functionalizing citrate-capped NPs through ligand exchange with oppositely charged ligands still presents challenges. Attempts to directly exchange the negatively charged citrate molecules of gold and silver NPs with positively charged ones often result in particle aggregation. This outcome is due to the citrate anions which act as a cross-linker through electrostatic interactions, and removing the citrate before exchange is not feasible without compromising the stability of NPs.[18] As a result, the cationization of citrate-coated NPs is a challenging task and, so far, a few studies have described the synthesis of cationic AuNPs using either a combination of double ligand exchange and a two-step phase transfer process[19] or ion exchange resins.[20] To date, the direct cationization of citrate-capped NPs through ligand exchange has not been reported.

Herein, we report a straightforward approach for functionalizing citrate-coated AuNPs (AuNPs-citrate) and citrate-coated AgNPs (AgNPs-citrate) with cationic ligands through a one-step ligand exchange method. Our approach involves controlling the protonation of negatively charged citrate molecules and simultaneously exchanging them with alkanethiols bearing positively charged terminal functionality. We demonstrate that the aggregation of negatively charged citrate-coated nanoparticles following the addition of positively charged ligands can be prevented by controlling the pH of the reaction environment.

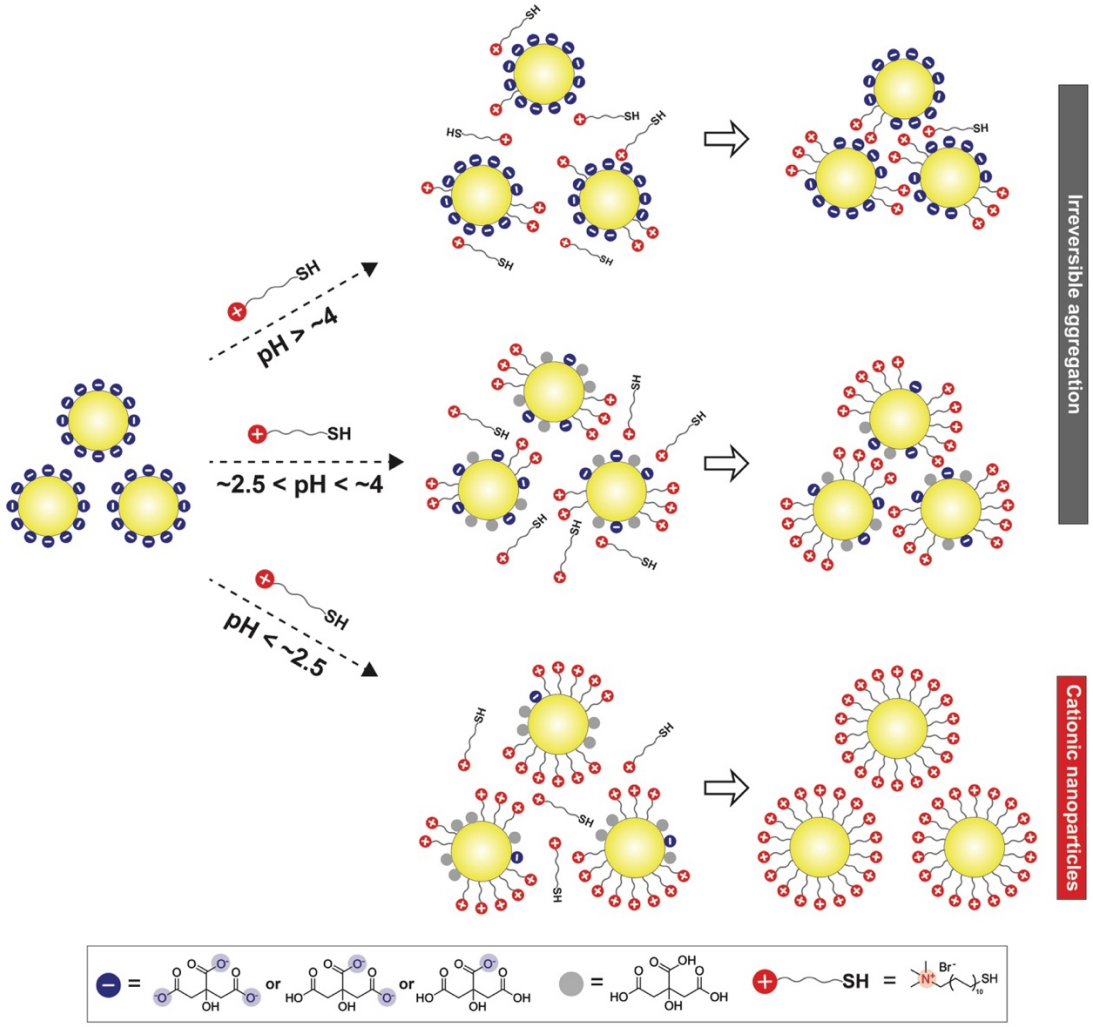

Figure 1. Schematic representation of the effect of pH on the ligand exchange process of citrate-coated nanoparticles with positively charged ligands.

As shown schematically in Figure 1, the lowering of pH leads to the protonation of citrate molecules, resulting in a reduction in the surface charge density of NPs. At high surface charge density, the addition of oppositely (positively) charged ligands leads to the aggregation of NPs, whereas this does not occur at low surface charge density. Under these conditions and exploiting the ability of thiol groups to bind to the metal nanoparticle surface strongly, it is feasible to exchange weakly bound citrate molecules with ligands featuring a positively charged functional group along with a thiol functional group, preventing aggregation and achieving well-dispersed positively charged NPs. We investigate the ligand exchange process of citrate-coated gold and silver nanoparticles with two alkanethiol ligands carrying positively charged terminal functionality, i.e. quaternary and primary

ammonium groups, through dynamic light scattering (DLS), zeta potential measurement, and transmission electron microscopy (TEM). Moreover, further insights into the ligand exchange mechanism and the dynamics of the process are provided by computational studies. Finally, to unveil the critical influence of nanoparticle surface charge on their interactions with biological systems, we explore their cytotoxic effects on both a fibroblast cell line and a colon cancer cell line.

Results and Discussion

Citrate-coated gold and silver nanoparticles with average diameters of 12 ± 1 nm and 20 ± 2 nm, as determined by transmission electron microscopy (TEM) analysis, and characteristic UV/Vis spectrum centered at 520 nm and 403 nm, respectively, were synthesized according to previously reported procedures (Figure S1).[7, 9] As shown in Figure 1, negatively charged citrate-coated nanoparticles were cationized by direct ligand exchange with positively charged ligands exploiting the proper pH conditions. AuNPs-citrate were rapidly added to aqueous solutions of (11-mercaptoundecyl)-N,N,N-trimethylammonium bromide (MUTAB) at different pH values (see Experimental section), and dynamic light scattering (DLS) was employed to monitor the hydrodynamic diameter. In Figure 2a, the hydrodynamic diameter values are reported as a function of pH after overnight incubation and washing (see Experimental section). As expected, the addition of AuNPs-citrate to the MUTAB solution without any pH correction (resulting in a final pH of ~6) led to the irreversible aggregation of the nanoparticles. However, when the pH of the ligand exchange process was lowered below approximately 4 by adding HCl to the MUTAB solution before mixing it with AuNPs-citrate, the aggregation became progressively less significant. As the pH decreases from approximately 4 to 2.5, the hydrodynamic diameter of aggregates undergoes a significant reduction from hundreds of nanometers to values comparable to the dimensions of AuNPs-citrate (dashed line in Figure 2a). This trend is also qualitatively confirmed by visual observation of the dispersions of NPs. While ligand exchange at pH values above 2.5 was accompanied by discoloration or a color change from red to purple of the gold dispersion, revealing aggregation, below pH 2.5, the color of

the dispersion remains as expected for a non-aggregate system (Figure 2a, inset). Furthermore, the UV/Vis spectrum of AuNPs-MUTAB clearly confirms that, when the final pH of the ligand exchange process was below 2.5, the aggregation of nanoparticles was negligible, as the profile shape of the spectrum is retained, and only a slight redshift (4 nm) of the maximum due to the change in refractive index is observed (Figure 2b, red line). Noteworthy, the absence of aggregation phenomena was further confirmed by the substantial invariance of the particle size distribution of AuNPs before and after ligand exchange of citrate molecules with the positively charged MUTAB (Figure 2c), as determined from the analysis of TEM images. In contrast, UV/Vis spectra of AuNPs-MUTAB obtained at higher pH values showed a broader surface plasmon band (Figure S2), indicating the formation of nanoparticle aggregates,[14] in agreement with the DLS data.

Finally, the cationization of AuNPs functionalized with MUTAB was confirmed by zeta potential measurements. In fact, after the ligand exchange of AuNPs-citrate with MUTAB at a pH lower than 2.5, a reversal of surface charge was observed from -41±1 mV for AuNPs-citrate to values greater than 30 mV for AuNPs-MUTAB (Data before and after the functionalization of AuNPs with MUTAB are summarized in Table S1).

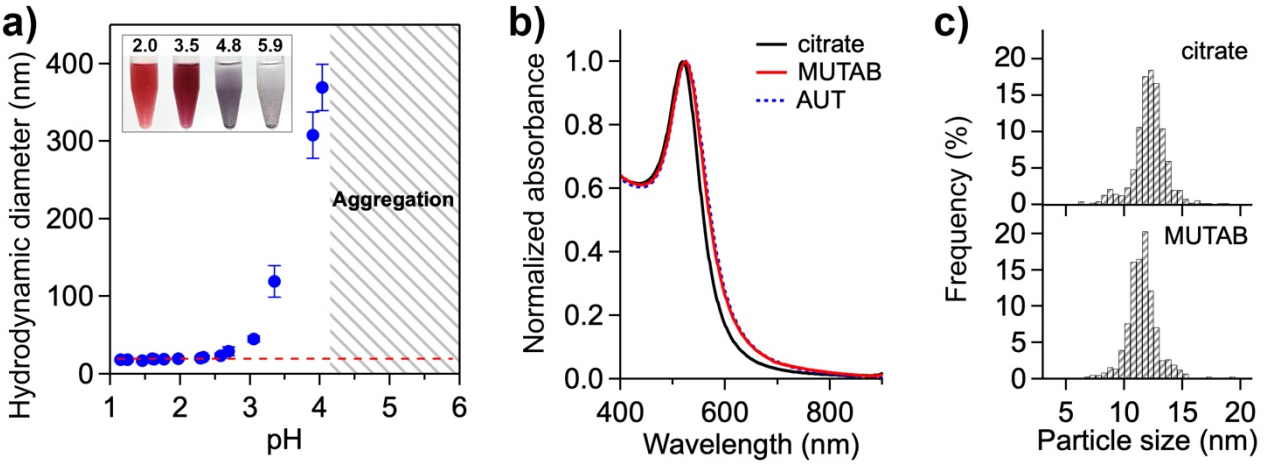

Figure 2. (a) Hydrodynamic diameter of AuNPs-citrate following ligand exchange with MUTAB as a function of pH conditions. Dashed line indicates the hydrodynamic diameter of the AuNPs-citrate. Inset: Photographs of AuNPs-citrate following ligand exchange with MUTAB at different pH values. (b) UV/Vis absorption spectra of citrate-, MUTAB- and AUT-coated AuNPs achieved at pH = 1.8. (c) Particle size distribution of citrate- and MUTAB-coated AuNPs achieved at pH = 1.8.

Besides MUTAB, cationization of AuNPs-citrate was also accomplished using a thiol-based ligand with a primary amine as the terminal group, specifically, 11-aminoundecanethiol hydrochloride (AUT). Direct ligand exchange of citrate molecules with AUT at a final pH below 2.5 resulted in positively charged AuNPs-AUT with a zeta potential of +31±2 mV and a UV/Vis spectrum overlapping with that of AuNPs-MUTAB (Figure 2b, blue line) (Data before and after the functionalization of AuNPs with AUT are summarized in Table S1).

As the successful cationization of AuNPs, we then also investigated the direct ligand exchange with AgNPs-citrate as a function of pH conditions. Similar to the observations with AuNPs, the ligand exchange of citrate-coated AgNPs with MUTAB, without pH correction, resulted in irreversible aggregation. However, when the pH was lowered by adding HCl to the MUTAB solution before mixing with the AgNPs, a significant reduction in aggregation phenomena occurred and at pH below 2.3-2.5 well-dispersed and positively charged AgNPs-MUTAB were successfully obtained (Figure S3). After the ligand exchange process, the UV/Vis spectrum profile of the AgNPs shows a slight redshift, with a maximum shift of 4 nm (Figure S4), and the zeta potential of the nanoparticles change from negative (-38±2 mV) to positive (+31±1 mV), confirming the successful direct cationization of AgNPs (Data before and after the functionalization of AgNPs with MUTAB are summarized in Table S1).

To shed light on the underlying mechanism of ligand exchange, we tried to measure the effect of pH decrease on the surface charge density of citrate-coated AuNPs by assessing the zeta potential. However, as previously reported, it is not possible to measure the zeta potential of AuNPs-citrate at pH levels lower than 5 due to the instability of the particles.[21] Therefore, we assessed the effect of pH on the stability of citrate-coated AuNPs by monitoring changes in their hydrodynamic diameter. As shown in Figure 3a, the pH titration of the citrate-coated AuNPs revealed the initiation of particle aggregation at pH levels below 2.5. According to the speciation diagram (Figure 3a inset), a decrease in pH leads to protonation of the three carboxyl groups and, for pH values below about 2.5, the fully

protonated (uncharged) form of citric acid (H_3Cit in Figure S6) becomes largely the predominant one, constituting more than 80% of the total molecules. As a result, the mean deprotonation state (α) at pH levels lower than 2.5 is less than 0.2 (see Figure S5), and a drastic decrease in the surface charge of AuNPs is therefore expected. We can infer that the instability of AuNPs at lower pH levels is due to the decrease in electrostatic repulsion, which is the main force stabilizing citrate-capped gold and silver nanoparticles.[14]

This conclusion is also supported by theoretical estimations of the overall surface charge (σ) of AuNPs based on the citrate coverage of the NP surface, which correlates with the α of citrate as calculated by the thermodynamic and coarse-grain model proposed by Franco-Ulloa *et al.*[22] According to this model, the surface coverage (ω_α) of AuNPs with citrate molecules varies with their deprotonation state, and thus with pH. Specifically, for single (α=1), double (α=2), and complete deprotonation (α=3) states, the citrate coverages are 0.01, 1.31, and 1.55 ligands per nm², respectively. These data, combined with the distribution of citrate's deprotonated states at varying pH levels, allows for the estimation of AuNPs' overall charge, as detailed in Figure 3b. When the value of α is below 0.4, corresponding to a pH of 3, the surface charge density falls below 0.02 e/nm^2. However, this surface charge would be too low to sustain sufficient electrostatic repulsions to prevent the AuNPs from aggregating, but DLS measurements show that at pH 3 the AuNPs are still stable (Figure 3a). We therefore deduced that the surface charge of NPs calculated by the model of Franco-Ulloa *et al.*[22] for α = 1 is underestimated, probably because it was designed specifically for the states α = 2 and α = 3. Therefore, we revisited the overall charge of AuNPs by adjusting the surface coverage for α=1 to 0.25× $\omega_{\alpha=3}$, yielding an estimated surface charge of about σ =0.2 e/nm^2 at pH 3. This fine-tuning aligns more precisely with the findings from DLS measurements, as it is observed that the surface charge of AuNPs lowers to near-zero levels at α values below 0.2, i.e. at pH values below 2.5 (Figure 3b, inset, blue dots).

Overall, the agreement between experimental data and theoretical predictions underscores the critical importance of reducing the surface charge density of NPs to allow direct ligand exchange of citrate-coated NPs with positively charged ligands.

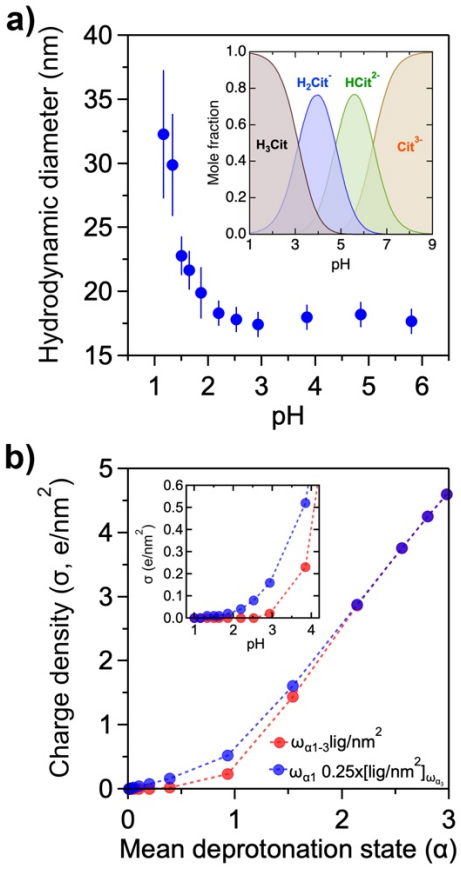

Figure 3. (a) Hydrodynamic diameter of AuNPs-citrate as a function of pH values. Measurements were performed immediately after the addition of 0.1 M HCl to AuNPs-citrate. Inset: Speciation diagram for citric acid ($pKa_1 = 3.13$; $pKa_2 = 4.76$; $pKa_3 = 6.40$ at 25°C). (b) AuNPs surface charge density (σ) versus the mean deprotonation state. Inset: AuNPs surface charge density (σ) versus pH. Data points for $\omega_{\alpha 1.3}$ (lig/nm²) calculated based on the model proposed by Franco-Ulloa *et al.*[22] and for a surface coverage for α=1 corresponding to $0.25\times\omega_{\alpha=3}$ are shown in blue and red, respectively.

Finally, we assessed the biological impact of varying the surface charge of the NPs on two cell lines, considering the well-known influence of surface coating on their biological effects. Our models included a fibroblast cell line (NIH-3T3) and a colon cancer cell line (HT-29). Both cell lines were exposed to a concentration of 30 µg/mL of nanoparticles, and their viability was evaluated after 48 hours using the MTT assay. As shown in Figure 4a, AuNPs exhibit moderate cytotoxic activity after

48 hours towards NIH-3T3 cell lines and any significant toxic effect with HT-29 cells, regardless of surface coating. These findings were further confirmed by optical images (Figure 4c-g), which show no significant differences between cells treated with NPs and those treated with vehicle solution (Figure S7). On one hand, both citrate-coated and MUTAB-coated AgNPs exhibit notable cytotoxicity on NIH-3T3 cells (Figure 4b), as also confirmed by optical images that showed a drastic decrease of cell density and impaired cell morphology (Figure 4g, h) compared to the control (Figure S7a). However, the situation changes when considering HT-29 cells, where the toxic effects vary significantly. As shown in Figure 4b, the viability of HT-29 cells treated with AgNPs-MUTAB falls below 60%, indicating a substantial decrease in cellular vitality compared to those treated with AgNPs-citrate, which remains unchanged compared to the control. The difference is clearly visible even from the optical images, where the density and morphology of HT-29 cells treated with AgNPs-citrate (Figure 4i) are similar to those of the control, while cells treated with AgNPs-MUTAB (Figure 4l) show significantly lower density and compromised cell morphology compared to the control (Figure S7b). Overall, these results not only confirm the inherent toxic activity difference between AuNPs and AgNPs under the same conditions, but also underscore the crucial influence of surface functionalization on the biological activity of nanoparticles.

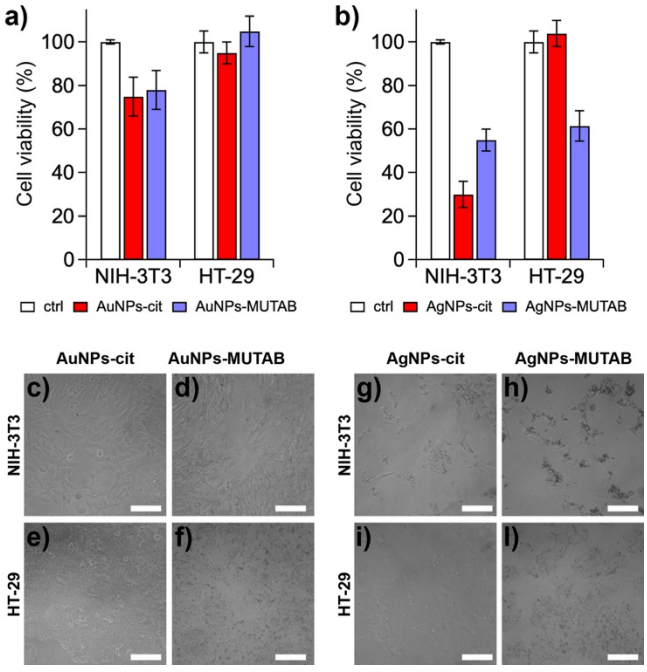

Figure 4. Cell viability of NIH-3T3 and HT-29 cells treated with (a) AuNPs and (b) AgNPs as a function of surface coating. Data represent the mean ± SD. Optical micrographs of NIH-3T3 cells treated with citrate- (c) and MUTAB-coated (d) AuNPs and HT-29 cells treated with citrate- (e) and MUTAB-coated (f) AuNPs. Optical micrographs of NIH-3T3 cells treated with citrate- (g) and MUTAB-coated (h) AgNPs and HT-29 cells treated with citrate- (i) and MUTAB-coated (l) AgNPs (scale bar 100 nm).

Conclusions

In conclusion, the successful cationization of citrate-coated gold and silver nanoparticles has been achieved through direct ligand exchange with positively charged ligands under specific pH conditions. By carefully controlling the pH throughout the exchange process, we effectively prevented nanoparticle aggregation, resulting in stable, positively charged nanoparticles. Through a comprehensive experimental and theoretical investigation, we shed light on the crucial role of pH in reducing the surface charge density of citrate-coated NPs, a key step to enable the direct addition of positively charged ligands, avoiding aggregation, and allowing ligand exchange. This dual approach allowed us to closely assess how changes in the protonation state of citrate molecules and alterations in surface charge dynamics influence the efficiency and outcome of ligand exchange on nanoparticles. Moreover, biological assays revealed varying cytotoxic effects of differently coated nanoparticles on fibroblast and cancer cell lines.

Overall, we present a straightforward strategy for obtaining cationic gold and silver nanoparticles without compromising their shape, stability, or functional properties. Additionally, we underscore the critical importance of surface functionalization in determining the biological impact of nanoparticles. This research not only offers valuable insights into nanoparticle functionalization and highlights their potential biomedical applications.

Experimental Section

Materials. Silver nitrate ($AgNO_3$), tetrachloroauric acid ($HAuCl_4 \cdot 3H_2O$), sodium citrate ($C_6H_5O_7Na_3$), tannic acid ($C_{76}H_{52}O_{46}$), (11-Mercaptoundecyl)-N,N,N-trimethylammonium bromide

(MUTAB), 3-(4,5- dimethyl-2-thiazolyl)-2,5-diphenyltetrazolium bromide (MTT), MEM Non Essential Amino Acids (NEAA), Dulbecco's phosphate buffered saline (DPBS) and Dulbecco's modified Eagle medium (DMEM) were purchased from Gibco and used without further purification. 11-aminoundecanethiol hydrochloride (AUT) was purchased from Prochimia Surfaces and used without further purification. Fetal bovine serum (FBS) was purchased from Gibco. All aqueous solutions were prepared with deionized water obtained using an ultrafiltration system (Milli-Q, Millipore) with a measured resistivity above 18 MΩ.

Synthesis of citrate-coated AuNPs. Citrate-stabilized AuNPs were prepared following the method reported elsewhere.[7] In brief, an aqueous solution of $HAuCl_4$ (100 mL, 1 mM) was refluxed for 5 min and an aqueous solution of sodium citrate (10 mL, 38.8 mM) was added quickly. Then, the reaction mixture was refluxed for 30 min, resulting in a deep red colloidal gold solution, and was then left to cool down to room temperature. The AuNPs-citrate were used as-prepared due to their instability to purification by centrifugation. The concentration, ca. 1×10^{13} particle mL^{-1}, was calculated according to previously reported extinction coefficients.[23]

Synthesis of citrate-coated AgNPs. Citrate-stabilized AgNPs were prepared following the method reported elsewhere.[9] In brief, 100 mL of aqueous solution of sodium citrate (5 mM) and tannic acid (0.025 mM) was refluxed and an aqueous solution of silver nitrate (1 mL, 25 mM) was added quickly. Then, the reaction mixture was refluxed for 15 min, resulting in a bright yellow colloidal silver solution, and was then left to cool down to room temperature. The aqueous suspension of AgNPs was purified by two rounds of centrifugation (30000g for 2h) and resuspension in 10 mL of aqueous solution of sodium citrate (2 mM) and then in deionized water. The final concentration of AgNPs, ca. 8×10^{12} particle mL^{-1}, was calculated according to previously reported extinction coefficients.[24]

Ligand exchange. In a plastic vessel, 1 mL of AuNPs-citrate was quickly added to 100 µL of a 2 mM aqueous solution of the ligand, which was previously acidified with 0.1 M HCl to achieve the desired final pH, and then left undisturbed overnight. The aqueous suspension of AuNPs was purified by two rounds of centrifugation (8000g for 20 min) and resuspension in 1 mL of deionized water.

Similarly, 0.1 mL AgNPs-citrate were quickly added to 100 µL of a 2 mM aqueous solution of ligand, which was previously acidified with 0.1 M HCl to achieve the desired final pH, and then left undisturbed overnight. The aqueous suspension of AuNPs was purified by two rounds of centrifugation (8000g for 20 min) and resuspension in 1 mL of deionized water.

Characterization of NPs. UV-Vis-NIR spectra were recorded on a Jasco V-550 UV/Vis spectrophotometer. Dynamic light scattering (DLS) and zeta potential measurement were performed in deionized water on a NanoBrook Omni Particle Size Analyser (Brookhaven Instruments Corporation, USA) equipped with a 35 mW red diode laser (nominal 640 nm wavelength). NPs were characterized using a Transmission Electron Microscopy (TEM) FEI TECNAI F20 ST, equipped with a dispersion micro-analysis of energy (EDS) and the Scanning Transmission Electron Microscopy (STEM) accessory. TEM samples were prepared by drop casting nanoparticle solutions onto a holey carbon-coated gold grid and dried at 80°C. The average size and size distribution of citrate-stabilized AgNPs were measured using ImageJ software by counting more than 800 particles. The TEM images were taken in the phase contrast mode and selected area electron diffraction (SAED). STEM pictures were recorded using High Angle Annular Dark Field (HAADF) detectors: in this imaging mode the intensity I is proportional to $Z^{1.7}t$, where Z is the mean atomic number and t is the thickness of the specimen.

Cell cultures. Human colon cancer cells, HT-29, were cultured under standard conditions in the DMEM medium supplemented with 10% (v/v) FBS, 2 mM L-glutamine, 100 U mL^{-1} of penicillin and 100 U mL^{-1} of streptomycin in a humidified incubator set at 37 °C with 5% CO_2. Mouse embryonic fibroblast cells, NIH-3T3, were cultured under standard conditions in the DMEM medium supplemented with 10% (v/v) heat-inactivated FBS, 2 mM L-glutamine, 0.1 mM MEM Non Essential Amino Acids (NEAA), 100 U mL^{-1} of penicillin and 100 U mL^{-1} of streptomycin in a humidified incubator set at 37 °C with 5% CO_2. The cells were seeded in 96-well plates at a concentration 5×10^4 cells per mL and grown for 24 h before exposure to nanoparticles. For the control, the cells were exposed to the vehicle solution.

Cell viability. Cell viability was determined by MTT assay measuring the intracellular reduction of tetrazolium salts into purple formazan by viable cells.[25] Briefly, the cells were seeded in 96-well plates and treated with NPs for 48h under standard conditions. After incubation, the medium with or without nanoparticles was discarded, and the cells were washed two times with DPBS. Afterwards, MTT solution (1 mg/mL) was added to each well and incubated for 1 h at 37 °C with 5% CO_2. The medium was discarded and formazan crystals were solubilized with DMSO. Optical density (OD) was read on a microplate reader (Thermo Scientific Varioskan Flash Multimode Reader) at 550 nm as a working wavelength and 640 nm as a reference. Cell viability was calculated as the proportion of the mean OD of the replicated wells relative to that of the control.

Corresponding Author

*denis.gentili@cnr.it (DG)

Notes

There are no conflicts to declare.

Acknowledgment

This work was supported by the Fondazione Cassa di Risparmio in Bologna (CARISBO) via bando Ricerca Medica e Alta Tecnologia 2023 (project No. 2023.0278). The authors would like to acknowledge Luana Mariani for the preliminary results and Federico Bona (CNR-ISMN) for valuable technical support.

References

1. Lohse, S. E.; Murphy, C. J., Applications of Colloidal Inorganic Nanoparticles: From Medicine to Energy. *J. Am. Chem. Soc.* **2012,** *134* (38), 15607-15620.
2. Yang, X.; Yang, M.; Pang, B.; Vara, M.; Xia, Y., Gold Nanomaterials at Work in Biomedicine. *Chem. Rev.* **2015,** *115* (19), 10410-10488.
3. Stark, W. J.; Stoessel, P. R.; Wohlleben, W.; Hafner, A., Industrial applications of nanoparticles. *Chem. Soc. Rev.* **2015,** *44* (16), 5793-805.

4. Gu, M.; Zhang, Q.; Lamon, S., Nanomaterials for optical data storage. *Nat. Rev. Mater.* **2016,** *1*, 16070.
5. Heuer-Jungemann, A.; Feliu, N.; Bakaimi, I.; Hamaly, M.; Alkilany, A.; Chakraborty, I.; Masood, A.; Casula, M. F.; Kostopoulou, A.; Oh, E.; Susumu, K.; Stewart, M. H.; Medintz, I. L.; Stratakis, E.; Parak, W. J.; Kanaras, A. G., The Role of Ligands in the Chemical Synthesis and Applications of Inorganic Nanoparticles. *Chem Rev* **2019,** *119* (8), 4819-4880.
6. Kang, H.; Buchman, J. T.; Rodriguez, R. S.; Ring, H. L.; He, J.; Bantz, K. C.; Haynes, C. L., Stabilization of Silver and Gold Nanoparticles: Preservation and Improvement of Plasmonic Functionalities. *Chem Rev* **2019,** *119* (1), 664-699.
7. Gentili, D.; Ori, G.; Ortolani, L.; Morandi, V.; Cavallini, M., Cooperative and Reversible Anisotropic Assembly of Gold Nanoparticles by Modulation of Noncovalent Interparticle Interactions. *ChemNanoMat* **2017,** *3* (12), 874-878.
8. Barbalinardo, M.; Caicci, F.; Cavallini, M.; Gentili, D., Protein Corona Mediated Uptake and Cytotoxicity of Silver Nanoparticles in Mouse Embryonic Fibroblast. *Small* **2018,** *14* (34), 1801219.
9. Barbalinardo, M.; Bertacchini, J.; Bergamini, L.; Magaro, M. S.; Ortolani, L.; Sanson, A.; Palumbo, C.; Cavallini, M.; Gentili, D., Surface properties modulate protein corona formation and determine cellular uptake and cytotoxicity of silver nanoparticles. *Nanoscale* **2021,** *13* (33), 14119-14129.
10. Decataldo, F.; Barbalinardo, M.; Gentili, D.; Tessarolo, M.; Calienni, M.; Cavallini, M.; Fraboni, B., Organic Electrochemical Transistors for Real-Time Monitoring of In Vitro Silver Nanoparticle Toxicity. *Adv. Biosys.* **2020,** *4* (1), 1900204.
11. Kimling, J.; Maier, M.; Okenve, B.; Kotaidis, V.; Ballot, H.; Plech, A., Turkevich Method for Gold Nanoparticle Synthesis Revisited. *J. Phys. Chem. B* **2006,** *110* (32), 15700-15707.
12. Bastús, N. G.; Comenge, J.; Puntes, V., Kinetically Controlled Seeded Growth Synthesis of Citrate-Stabilized Gold Nanoparticles of up to 200 nm: Size Focusing versus Ostwald Ripening. *Langmuir* **2011,** *27* (17), 11098-11105.
13. Hühn, J.; Carrillo-Carrion, C.; Soliman, M. G.; Pfeiffer, C.; Valdeperez, D.; Masood, A.; Chakraborty, I.; Zhu, L.; Gallego, M.; Yue, Z.; Carril, M.; Feliu, N.; Escudero, A.; Alkilany, A. M.; Pelaz, B.; del Pino, P.; Parak, W. J., Selected Standard Protocols for the Synthesis, Phase Transfer, and Characterization of Inorganic Colloidal Nanoparticles. *Chem. Mater.* **2016,** *29* (1), 399-461.
14. Gentili, D.; Ori, G., Reversible assembly of nanoparticles: theory, strategies and computational simulations. *Nanoscale* **2022,** *14* (39), 14385-14432.
15. Al-Johani, H.; Abou-Hamad, E.; Jedidi, A.; Widdifield, C. M.; Viger-Gravel, J.; Sangaru, S. S.; Gajan, D.; Anjum, D. H.; Ould-Chikh, S.; Hedhili, M. N.; Gurinov, A.; Kelly, M. J.; El Eter, M.; Cavallo, L.; Emsley, L.; Basset, J.-M., The structure and binding mode of citrate in the stabilization of gold nanoparticles. *Nat. Chem.* **2017,** *doi:10.1038/nchem.2752*.
16. Bastus, N. G.; Merkoci, F.; Piella, J.; Puntes, V., Synthesis of Highly Monodisperse Citrate-Stabilized Silver Nanoparticles of up to 200 nm: Kinetic Control and Catalytic Properties. *Chem. Mater.* **2014,** *26* (9), 2836-2846.
17. Rycenga, M.; Cobley, C. M.; Zeng, J.; Li, W.; Moran, C. H.; Zhang, Q.; Qin, D.; Xia, Y., Controlling the Synthesis and Assembly of Silver Nanostructures for Plasmonic Applications. *Chem. Rev.* **2011,** *111* (6), 3669-3712.
18. Ojea-Jiménez, I.; Puntes, V., Instability of Cationic Gold Nanoparticle Bioconjugates: The Role of Citrate Ions. *J. Am. Chem. Soc.* **2009,** *131* (37), 13320-13327.
19. Hassinen, J.; Liljestrom, V.; Kostiainen, M. A.; Ras, R. H. A., Rapid Cationization of Gold Nanoparticles by Two-Step Phase Transfer. *Angew. Chem. Int. Ed.* **2015,** *54* (27), 7990-7993.
20. Ishida, Y.; Suzuki, J.; Akita, I.; Yonezawa, T., Ultrarapid Cationization of Gold Nanoparticles via a Single-Step Ligand Exchange Reaction. *Langmuir* **2018,** *34* (36), 10668-10672.
21. Brewer, S. H.; Glomm, W. R.; Johnson, M. C.; Knag, M. K.; Franzen, S., Probing BSA Binding to Citrate-Coated Gold Nanoparticles and Surfaces. *Langmuir* **2005,** *21* (20), 9303-9307.

22. Franco-Ulloa, S.; Tatulli, G.; Bore, S. L.; Moglianetti, M.; Pompa, P. P.; Cascella, M.; De Vivo, M., Dispersion state phase diagram of citrate-coated metallic nanoparticles in saline solutions. *Nat. Commun.* **2020,** *11* (1), 5422.
23. Liu, X. O.; Atwater, M.; Wang, J. H.; Huo, Q., Extinction coefficient of gold nanoparticles with different sizes and different capping ligands. *Colloids Surf. B* **2007,** *58* (1), 3-7.
24. Paramelle, D.; Sadovoy, A.; Gorelik, S.; Free, P.; Hobley, J.; Fernig, D. G., A rapid method to estimate the concentration of citrate capped silver nanoparticles from UV-visible light spectra. *Analyst* **2014,** *139* (19), 4855-4861.
25. Twentyman, P. R.; Luscombe, M., A study of some variables in a tetrazolium dye (MTT) based assay for cell growth and chemosensitivity. *Br. J. Cancer* **1987,** *56* (3), 279-285.